CuO-CeO$_2$ supported on montmorillonite-derived porous clay heterostructures (PCH) for preferential CO oxidation in H$_2$-rich stream

J.A. Cecilia [a], A. Arango-Díaz [a], F. Franco [a], J. Jiménez-Jiménez [a], L. Storaro [b], E. Moretti [b,∗], E. Rodríguez-Castellón [a,∗]

[a] *Departamento de Química Inorgánica, Facultad de Ciencias, Universidad de Málaga, 29071 Málaga, Spain*
[b] *Department of Molecular Sciences and Nanosystems, Ca' Foscari University of Venice, INSTM Venice Research Unit, Via Torino 155/B, 30172 Venice, Italy*

ARTICLE INFO

ABSTRACT

This study reports on the preparation and characterization of porous clay heterostructures (PCH) as a high-surface-area support for CuO–CeO$_2$ based catalysts for the preferential oxidation of CO in excess of H$_2$ (CO-PROX). After pillaring the montmorillonite clay with silica (Si-PCH) and silica-zirconia (SiZr-PCH), the Cu-Ce active phase was loaded by incipient wet impregnation setting the cerium amount constant (20 wt%) and investigating three different copper loadings (3, 6 and 12 wt%). The use of pillars of silica or silica-zirconia inserted in the interlayer space of a natural clay provides a high surface area support that can favor the dispersion of both CuO and CeO$_2$ active phases, leading to the formation of a high amount of copper-ceria interfacial sites, responsible for a very high catalytic activity in the CO-PROX reaction.

The results obtained from characterization of the materials by XRD, N$_2$ physisorption, H$_2$-TPR, XPS and CO$_2$-TPD suggest that this synthesis method gives rise to catalysts with copper species highly active and selective for the CO-PROX reaction.

The catalysts exhibit high CO conversion values and the sample with 6 wt% of copper on Si-PCH displays very good performances, comparable to those based on precious metal catalysts, even at low temperatures.

The system reducibility was found modified by the incorporation of zirconium in the support, with a slight decrement of the CO conversion value, compared to the same material without Zr. The influence of the presence of CO$_2$ and H$_2$O in the gas feed was also studied in order to simulate the real operating conditions of a PEMFC feed stream. Correlations between catalytic performances and physicochemical properties of the materials have been made.

© 2015 Elsevier B.V. All rights reserved.

1. Introduction

The low-temperature proton exchange membrane fuel cells (PEMFCs) have been largely studied and developed during the last two decades especially due to their low temperature of operation (about 80 °C), high power density, high efficiency and the environmentally benign nature. PEMFC technology promises to be a clean and efficient alternative to combustion of fuels for power generation in stationary and mobile applications [1]. Hydrogen, as PEMFC fuel, can be generated by steam reforming, partial oxidation, or auto-thermal reforming of liquid fuels [2] or natural gas in combination with the water gas shift reaction. However, the anode catalysts of the cell have demonstrated to be easily poisoned by traces of CO (even around 1 ppm). Therefore it is necessary to eliminate the traces of CO in the hydrogen stream with minimum hydrogen consumption. For this purpose, several methods for CO removal from the hydrogen stream have been reported in the literature [3] and, among them, the preferential oxidation of carbon monoxide (CO-PROX) seems to be the most straightforward and cost-effective method to achieve acceptable CO concentrations [4–6].

The challenges involved in the design of successful CO-PROX catalysts are related with the increase of the activity at low temperatures and the selectivity towards the oxidation of CO against the undesired H$_2$ oxidation that decreases the overall process efficiency and finally a good resistance to deactivation, caused by the presence of H$_2$O and CO$_2$ in the feed.

Catalysts reported for CO-PROX reaction are mainly precious metal catalysts, such as Pt [7,8], Pd [9], Au [10,11], Ru [12,13] or Rh [14,15], which exhibit a high conversion values at low temperature.

∗ Corresponding authors. Tel.: +39 0412346745; fax: +39 0412346735.
E-mail addresses: elisa.moretti@unive.it (E. Moretti), castellon@uma.es (E. Rodríguez-Castellón).

However, due to the high cost and limited availability the development of new catalytic systems more abundant and less expensive is necessary. In this sense, non-precious metal based catalysts are considered as promising alternatives and catalysts based on the closely interacting $CuO-CeO_2$ have been purposed as promising for the CO-PROX reaction for their high activity, selectivity and relatively low cost [16–29]. For copper-ceria system, the establishment of an intimate contact between both components produces a promoting effect for ceria with fluorite-type structure, responsible of the high oxygen mobility [30,31] leading to both change in redox state capacity and bifunctional promotion. This behavior generates a synergistic effect between copper oxide clusters and ceria, where Cu^+ species are stabilized providing surface sites for CO adsorption, while cerium oxide provides oxygen vacancies. Thereafter, the redox process for the CO oxidation produces the reduction and oxidation of both the copper and ceria phases [32]. The redox behavior of $CuO-CeO_2$ systems can be enhanced by the incorporation of heteroatoms as zirconium, which can improve the oxygen storage capacity by the increase of defects in the framework [27,33,34]. Moreover ceria and ceria/zirconia finely dispersed on Al_2O_3 as support were described. This support was found to favor an intimate contact between Al_2O_3 and the highly dispersed CeO_2 particles, facilitating the interaction between them [35].

Commonly, copper-ceria oxide systems described for CO-PROX have been classified into three kinds, i.e., CuO/CeO_2, inverse CeO_2/CuO and supported $CuO-CeO_2$, being CuO/CeO_2 the more studied system. With regards to the supported ones, mesoporous silicas have been extensively investigated in the catalysis field because of its well-ordered porosity and large surface area, however, the use of supported $CuO-CeO_2$ have been only limited to a few mesoporous silicas as HMS, SBA-15, SBA-16 and MCM-41 as supports for CO-PROX reaction [12,36–38].

The modification of the interlayer space of the smectite by the insertion of the polyoxocations species (PILC), for the obtention of materials with interesting textural properties, has found a wide range of applications in catalysis, adsorption and separation processes. Al-PILC has been employed as support for $CuO-CeO_2$ catalysts showing a good performance in CO-PROX [39].

The present paper is concerned with the possibility of using porous clay heterostructures (PCH) as support for $CuO-CeO_2$ based catalysts. The synthetic methodology for the PCH materials, described by Galarneau et al. [40], allows obtaining porous solids based on cationic layered clays by the formation of silica pillars intercalated between clay layers. Control of the pillaring process is a very promising means to obtain solids with high surface area and a broad spectrum of structural, chemical and catalytic properties. Moreover these materials exhibit a higher thermal stability than PILC [41]. The chemical properties of PCHs can be modified by the incorporation of heteroatoms such as Al [42] or Zr [43,44] into the siliceous framework of the PCHs. The use of PCHs as support for copper-ceria oxides based catalysts can increase the dispersion of the active phase due to the high surface area of support that can offer a high activity in CO-PROX reaction. For this purpose, a PCH with silica pillars and a PCH with silica-zirconia pillars were synthesized as supports to study the catalytic behavior of $CuO-CeO_2$ systems in the CO-PROX reaction.

2. Materials and methods

2.1. Materials

The raw material used for the synthesis of PCHs was a bentonite from "Serrata de Níjar", southeast Spain, which was supplied by Minas de Gador S.A. Chemicals employed to prepare the PCHs were cetyltrimethylammonium bromide (CTMBr, Aldrich), anhydrous

n-propanol (99.9%, VWR), hexadecylamine (Aldrich), tetraethylorthosilicate (98% Aldrich) and zirconium(IV) propoxide (70% solution *n*-propanol) (Aldrich). The reagents used to prepare the catalytic precursors were copper(II) acetate monohydrate (>99% Aldrich) and cerium(III) acetate hydrate (99.9% Aldrich). The gases evolved in the characterization and catalytic tests were He (Air Liquide 99.99%), N_2 (Air Liquide 99.9999%), H_2 (Air Liquide 99.999%), CO_2 (Air Liquid 99.999%), O_2/N_2 (20/80, % vol.) (Aldrich 99.999%), H_2/Ar, 10%. vol. (Air Liquide 99.99%) O_2/He, 5% vol. (Air Liquide 99.9%) and CO/He, 10% vol. (Linde 99.9%).

2.2. Preparation of catalysts

The raw bentonite, used for the synthesis of PCH, was previously characterized [45,46]. The largest (> 90 wt%) mineralogical component of this bentonite is montmorillonite. In order to purify the raw material, the montmorillonite fraction of bentonite was collected by conventional sedimentation and stirred in a 1 M NaCl solution, during 1 day, to obtain Na–montmorillonite. This clay, used as a starting material, had a BET surface area of 99 $m^2 g^{-1}$.

Both Si-PCH and SiZr-PCH samples, with Si/Zr molar ratio of 5, were prepared according to the method proposed by Cecilia et al. [44]. The active phase was incorporated into the support by incipient wetness impregnation using an aqueous solution of copper(II) and cerium(III) acetates. All catalysts were prepared with a loading of 20 wt% of cerium and a loading ranging from 3 to 12 wt% of copper. All samples were dried for 12 h at 60 °C and then calcined at 400 °C for 4 h with a heating ramp of 1 °C min^{-1}. The catalysts were denoted as Si-*x*Cu*y*Ce and SiZr-*x*Cu*y*Ce, where *x* and *y* represent the percentage by weight of copper and cerium in the sample, respectively. After CO-PROX catalytic tests, the samples were denoted as Si-*x*Cu*y*Ce-U and SiZr-*x*Cu*y*Ce-U, where *U* means "used".

2.3. Characterization methods

The purified bentonite was examined by scanning electron microscope (SEM) using a JEOL SM-6490 LV combined with X-ray energy dispersive spectroscopy (EDX). The samples were goldsputtered in order to avoid charging of the surface. Elemental composition of the bentonite was achieved by the average of EDX chemical analyses of 40 grains.

X-ray powder patterns for the samples were collected on a X'Pert Pro MPD automated diffractometer (PANalytical B.V.) equipped with a Ge(111) primary monochromator (strictly monochromatic CuKα_1 radiation) and an X'Celerator detector with a step size of 0.017°. The powder patterns were recorded between 10° and 70° in 2θ with a total measuring time of 30 min. Low angle measurements were obtained with the same configuration maintaining the divergence and anti-divergence aperture at 1/16° and with Soller of 0.02 rad. Measurements were carried out from 0.5–10° in 2θ with a step size of 0.017°.

In order to determine the carbon content present after the calcinations of the template, after the combustion of the samples at 1100 °C in pure oxygen to form CO_2, elemental chemical analysis was performed using a LECO CHN 932 analyzer.

The textural parameters were evaluated from nitrogen adsorption–desorption isotherms at −196 °C as determined by an automatic ASAP 2020 system from Micromeritics. Prior to the measurements, samples were outgassed at 200 °C and 10^{-4} mbar overnight. Specific surface areas (S_{BET}) were determined by using the Brunauer–Emmett–Teller (BET) equation and a nitrogen molecule cross section of 16.2 A^2 [47]. The pore size distribution was calculated by applying the Barret–Joyner–Halenda (BJH) method to the desorption branch of the N_2 isotherm [48]. The total pore volume (V_P) was calculated from the adsorption isotherm at $P/P_0 = 0.98$.

Hydrogen temperature-programmed reduction (H_2-TPR) experiments were carried out to 0.080 g of catalyst precursor, previously treated with a He flow (35 ml min^{-1}) at 100 °C for 30 min. After cooling to room temperature, the H_2 consumption was studied between this temperature and 800 °C, by using an Ar/H_2 flow (48 ml min^{-1}, 10 vol% of H_2) and under a heating rate of 10 °C min^{-1}. Water formed in the reduction reaction was removed by means of an isopropanol-liquid nitrogen trap and a cold finger (−80 °C). The H_2 consumption was measured with an on-line gas chromatograph (Shimadzu GC-14A) provided with a TCD. The hydrogen consumption was quantified by calibration with pure CuO as reference compound (Aldrich).

X-ray photoelectron spectra were collected using a Physical Electronics PHI 5700 spectrometer with non-monochromatic Mg Kα radiation (300 W, 15 kV, and 1253.6 eV) with a multi-channel detector. Spectra of pelletized samples were recorded in the constant pass energy mode at 29.35 eV, using a 720 μm diameter analysis area. Charge referencing was measured against adventitious carbon (C 1s at 284.8 eV). A PHI ACCESS ESCA-V6.0 F software package was used for acquisition and data analysis. A Shirley-type background was subtracted from the signals. Recorded spectra were always fitted using Gaussian–Lorentzian curves in order to determine the binding energies of the different element core levels more accurately. The error in BE was estimated to be ca. 0.1 eV. A short acquisition time of 10 min was used to examine C 1s, Cu 2p and Cu LMM XPS regions in order to avoid, as much as possible, photoreduction of Cu^{2+} species. Nevertheless, a Cu^{2+} reduction in high vacuum during the analysis cannot be excluded [49].

The CO_2 desorption of the catalysts was studied by temperature-programmed desorption of CO_2. Approximately 100 mg of each sample was pretreated with a stream of air at 400 °C for 30 min (10 °C min^{-1} and 60 ml min^{-1}). The reaction temperature was then decreased to 40 °C, and a flow of pure CO_2 (60 ml min^{-1}) was subsequently introduced into the reactor for 30 min. The CO_2-TPD reaction was carried out between 40 and 400 °C under a He flow (10 °C min^{-1}, 30 ml min^{-1}), and the amount of CO_2 evolved was analyzed using a quadrupole mass spectrometer (Balzer GSB 300 02) equipped with a Faraday detector (0–200 U), which monitors the mass of CO_2 (44 U) during the experiment.

2.4. Catalytic tests

Catalytic tests were carried out in a fixed bed reactor at atmospheric pressure. The catalysts (0.150 g), with a particle size (0.050–0.110 mm) were introduced into a tubular stainless steel reactor (5 mm i.d.) controlled by interior place thermocouple in direct contact with the catalysts. The samples were pre-treated in-situ under flowing air for 30 min at 400 °C, followed by cooling to room temperature in He flow. The contact time W/F was 0.18 g s cm^{-3} (GHSV = 22000 h^{-1}). The reaction mixture composition was 1.25% CO, 1.25% O_2, 50% H_2, balanced with He. The effect of CO_2 and H_2O was examined with the addition of 15% CO_2 and 12% H_2O. An ice-salt cooled cold finger (−20 °C) was used to trap the water downstream from the reactor. A Shimadzu-GC-2014 gas chromatograph equipped with TCD, with a CP-Carboplot-P7 column, was used to analyze the outlet composition. The detector limit for CO was 10 ppm. The temperature was varied in the 65–190 °C range and measurements were carried out till a steady state was achieved.

The carbon monoxide (Eq. (1)) and oxygen (Eq. (2)) conversions were calculated based on the CO and O_2 consumption, respectively:

$$CO\ conversion(\%) = \frac{n_{CO}^{in} - n_{CO}^{out}}{n_{CO}^{in}} \times 100 \qquad (1)$$

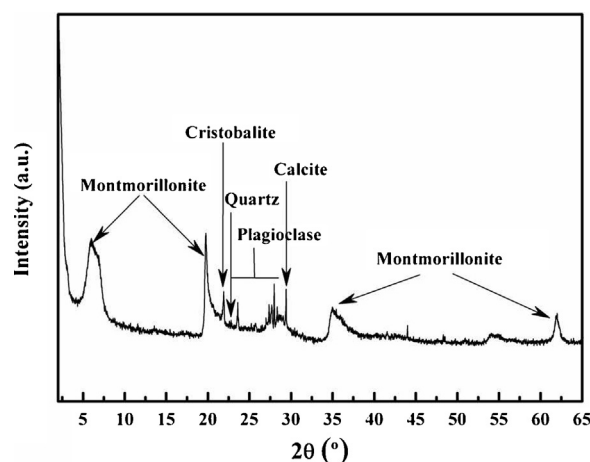**Fig. 1.** XRD profile of raw bentonite (mineralogical identification).

$$O_2\ conversion(\%) = \frac{n_{O_2}^{in} - n_{O_2}^{out}}{n_{O_2}^{in}} \times 100 \qquad (2)$$

where n represents the inlet (in) and outlet (out) concentrations.

The selectivity towards CO_2 was calculated by (Eq. (3)):

$$CO_2\ selectivity(\%) = \frac{1}{\lambda} \frac{x_{CO}}{x_{O_2}} \times 100 \qquad (3)$$

The excess oxygen factor (λ) is defined as (Eq. (4)):

$$\lambda = 2 \times \frac{n_{O_2}^{in}}{n_{CO}^{in}} \qquad (4)$$

The excess oxygen factor (λ) used was 2 because this value was previously found optimal for CO-PROX [29,50].

3. Results and discussion

3.1. Characterization of catalysts

3.1.1. Elemental analysis

On the basis of the elemental analysis of the Na-Montmorillonite, obtained by the average of EDX chemical analysis of 40 grains, the resulting structural formula is:

$(Na_{0.8})(Al_{3.3}Mg_{0.5}Fe_{0.2})^{VI}(Si_{7.7}Al_{0.3})^{IV}O_{20}(OH)_4$ where "VI" and "IV" indicate the location of the different cations in metal oxide octahedrons or tetrahedrons, respectively. Aluminum was assigned to tetrahedral positions to complete an occupancy of eight, then magnesium and iron were assigned to octahedral sites and completed an occupancy of four, sodium ions were assigned to the interlayer.

The resulting formula represents a Wyoming-type montmorillonite, according to the classification by Schultz [51] because of the layer charge, lower than 0.85 electron charges per unit cell (e$^-$/u.c.), and the percentage of tetrahedral substitution.

3.1.2. X-ray diffraction

X-ray diffractogram of raw bentonite shows that the main mineralogical component is montmorillonite (>90%) together with minor amounts of plagioclase, cristobalite, calcite and almost undetectable presence of quartz (Fig. 1). After pillared process, XRD patterns of both Si-PCH and SiZr-PCH show a broad peak at low angle (Fig. 2A), corresponding to the d_{001} lattice spacing which suggests the formation of an expanded structure of the original montmorillonite where the pillars keep separated and strongly bound the adjacent sheets and delimit a great number of galleries between them [40]. The inclusion of zirconium in the pillars
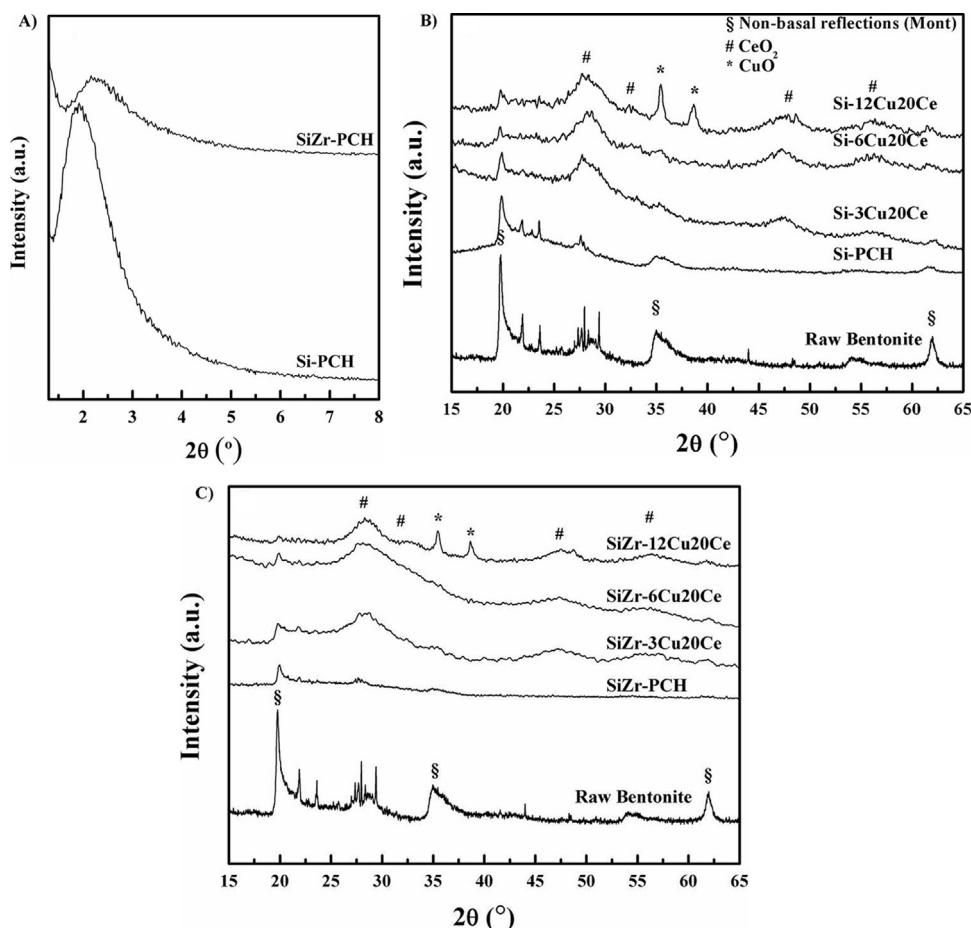
Fig. 2. X-Ray diffractograms: (A) at low angle of Si-PCH and SiZr-PCH; (B) at high angle of Si-*x*Cu*y*Ce samples; (C) at high angle of SiZr-*x*Cu*y*Ce catalysts.

produces a shift of the d_{001} diffraction line to higher 2θ angle, becoming broader and smaller due to a strong delamination process that leads to a more disorder structure denoted as "house of card like" [44].

When the pillars of silica and silica-zirconia are inserted in the interlayer space of montmorillonite (Fig. 2B–C), the basal reflections disappear, while the non-basal reflections of montmorillonite (020, 110, 200, 060) suffer a decrease of its intensity, revealing a structural change along the c^*-ax due to the formation of pillars in the interlayer space of the smectite [44].

The incorporation of copper and cerium species to the PCHs by impregnation leads to a partial degradation of the porous framework due to the high loading content of the active phases. XRD diffractograms (Fig. 2B–C) display broad diffraction lines at $2\theta = 28.5$, 33.4, 47.5 and 56.5° which have been attributed to cubic fluorite CeO$_2$ (PDF-ICCD 00-034-0394) indicating that cerianite phase exhibits a small particle size and a high dispersion in both Si-PCH and SiZr-PCH samples. As expected, no characteristic peaks due to crystalline copper oxide phase were observed in the 34–40° range for the catalysts with 3 wt% of copper loading (Si-3Cu20Ce and SiZr-3Cu20Ce), indicating the absence of bulk CuO in these two samples. No signal attributable to copper species were detected neither in the XRD profiles of the samples with 6 wt% of Cu, suggesting that the active phase is highly dispersed on the pillared supports. Anyway, owing to the small size of Cu^{2+} ion, the presence of copper in solid solution or as interstitial punctual defects in the ceria lattice cannot be ruled out. The presence of copper species is noticeable in Si-12Cu20Ce and SiZr-12Cu20Ce samples,

which exhibit diffraction lines at 35.5 and 38.6° of 2θ, assigned to monoclinic CuO (tenorite phase, PDF-ICCD 00-048-1548).

3.1.3. N$_2$ physisorption

To disclose the textual characteristic of the prepared catalysts, N$_2$ physisorption measurements at $-196\,°C$ were performed. Data of the bare montmorillonite, Si-PCH and SiZr-PCH catalysts are reported in Table 1. The incorporation of silica and silica-zirconia into the montmorillonite clay provoked in every case a change in the isotherm profiles. According to the IUPAC classification [52] and refined by Rouquerol et al. [53], bentonite shows an isotherm of type II. After pillaring with silica and silica-zirconia both PCHs exhibit a combination of type I and type IIb isotherms: the former associated to the presence of microporosity and the latter with monolayer-multilayer adsorption on an open and stable external surface of a powder with macroporosity (Fig. 3A). These isotherms are obtained with aggregates of plate-like particles, which therefore possess non-rigid slit-shaped pores. Both PCHs present a narrow H3 type hysteresis loops with no indication of a plateau at high P/P_0, which are typically found on solids consisting of aggregates or agglomerates of particles forming slit shaped pores (plates or edged particles like cubes). The incorporation of zirconium to form the PCH materials produces a shrinkage of the hysteresis loop, suggesting the presence of blind cylindrical, cone-shaped and wedge-shaped pores [52] which is commonly related with the house of cards packing of extremely delaminated clay minerals [54]. The addition of zirconium in the synthesis of PCH leads to a more disordered structure.

Table 1
Textural parameters of Si-xCuyCe and SiZr-xCuyCe catalysts.

Sample	S_{BET} (m² g⁻¹)	S_{microp} (m² g⁻¹)[a]	V_p (cm³ g⁻¹)	V_{microp} (cm³ g⁻¹)[a]
Montmorillonite	99	18	0.19	0.01
Si-PCH	571	392	0.75	0.21
Si-3Cu20Ce	418	268	0.68	0.13
Si-6Cu20Ce	328	209	0.48	0.11
Si-12Cu20Ce	285	187	0.45	0.09
SiZr-PCH	550	372	0.82	0.21
SiZr-3Cu20Ce	484	257	0.72	0.14
SiZr-6Cu20Ce	316	179	0.53	0.09
SiZr-12Cu20Ce	279	171	0.36	0.08

[a] S_{microp} and V_{microp} were estimated by t-plot method.

The specific surface area was calculated using the BET method. Both PCH supports show a rise of the S_{BET} from 99 m² g⁻¹ for the bare montmorillonite to 572 m² g⁻¹ for Si-PCH and 550 m² g⁻¹ for SiZr-PCH by the insertion of pillars between the 2:1 layers of montmorillonite (Table 1). The introduction of ceria-copper oxide system to the PCHs produces a decrease in surface area and cumulative pore volume due to a partial blockage, mainly of the microporous framework (Fig. 3B–C and Table 1). Despite these textural parameters decrease with the increasing of CuO-CeO₂ loading, our catalysts supported on PCHs exhibit a higher surface area than the bulk CuO-CeO₂ systems reported in the literature, favoring the presence of a higher amount of active centers with a noteworthy dispersion as shown by XRD diffractograms (Fig. 2B–C).

3.1.4. H_2-TPR

The H_2-Temperature Programmed Reduction (H_2-TPR) profiles of the fresh calcined samples with different copper and cerium content are displayed in Fig. 4A–B, while the H_2 consumption values and the exceeding the stoichiometric ones (H_2/Cu molar ratio) for all the samples are reported in Table 2. The analysed samples showed quite complex H_2-TPR profiles, reflecting the heterogeneity of the existing copper species.

Redox behavior of copper-ceria oxide based catalysts and the correlation between redox and catalytic behavior have been widely accepted due the interactions between CuO and CeO₂ in the interface sites [24]. The reduction of pure CuO powder typically takes place in the temperature range 320–380 °C, while pure CeO₂ undergoes reduction in the range 450–850 °C, generally with two temperature maxima due to the reduction of surface Ce⁴⁺ followed by reduction of bulk ceria, respectively [55]. However, for copper-ceria oxide systems the temperature reduction is shifted at lower temperature between 150 and 300 °C, which indicates an increasing of the reducibility of the catalytic system by the synergistic effect in the interface sites of CuO-CeO₂ system [56].

When the CuO-CeO₂ system is supported on Si-PCH, the reduction process takes place between 120 and 290 °C and the quite complex profile can be deconvolved in four main peaks in accordance with Ayastuy et al. [20]. The investigated samples exhibit a four-step reduction, where the first peak (denoted α_1) at lower temperature has been ascribed to the reduction of isolated Cu²⁺
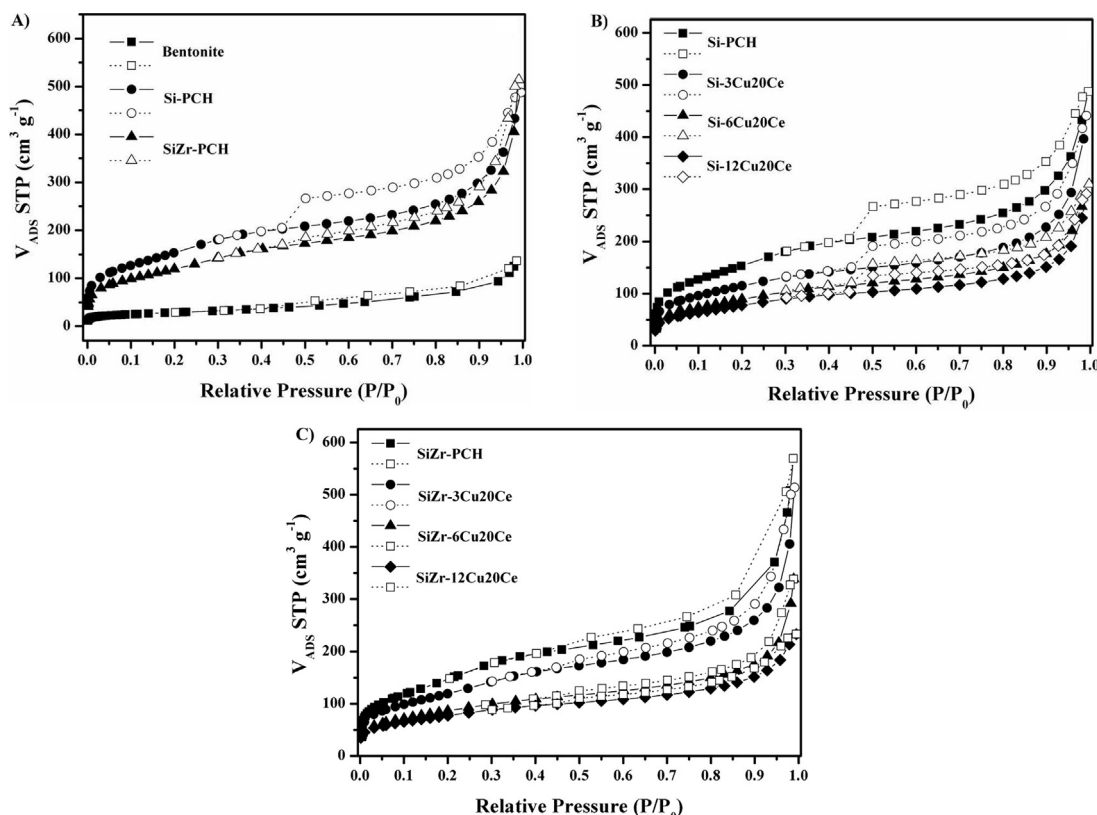

Fig. 3. N₂ isotherms at −196 °C of: (A) bare montmorillonite and montmorillonite-derived PCHs; (B) Si-xCuyCe and (C) SiZr-xCuyCe samples.
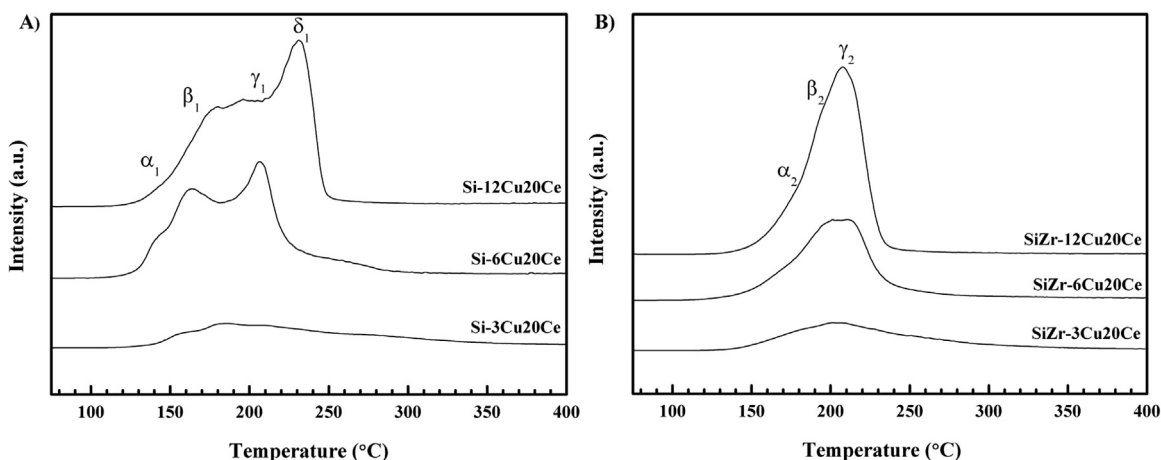
Fig. 4. H_2-TPR profiles of: (A) Si-xCuyCe and (B) SiZr-xCuyCe catalysts.

Table 2
Reducibility degree, obtained by H_2-TPR, for Si-xCuyCe and SiZr-xCuyCe catalysts.

Sample	α_1 (%)	β_1 (%)	γ_1 (%)	δ_1 (%)	H_2 uptake (μmol g^{-1})	H_2/Cu (mol/mol)
Si-3Cu20Ce	9.6	36.2	39.1	15.1	705	1.87
Si-6Cu20Ce	6.5	39.1	50.3	4.1	1246	1.65
Si-12Cu20Ce	3.7	25.6	23.6	47.2	2159	1.43
	α_2 (%)	β_2 (%)	γ_2 (%)	δ_2 (%)	H_2 uptake (μmol g^{-1})	H_2/Cu (mol/mol)
SiZr-3Cu20Ce	8.1	40.7	51.2	–	803	2.13
SiZr-6Cu20Ce	6.7	45.3	48.0	–	1412	1.87
SiZr-12Cu20Ce	6.4	46.1	47.5	–	2446	1.62

species, which interact strongly with ceria. The second step (β_1 peak) has been assigned to the reduction of dispersed Cu^{2+} species in close contact with CeO_2 surface. The third step (γ_1 peak) can be ascribed to the reduction of small clusters of copper oxide without specific and regular lattice arrangement and CuO in solid solution in the ceria lattice and finally the fourth peak (δ_1 peak) has been assigned to the reduction of larger clusters and bulk-like CuO species that are loosely bound to ceria on the support. H_2-TPR profiles of the samples Si-PCH supported (Fig. 4A and Table 2) show that Si-3Cu20Ce and Si-6Cu20Ce have the same amount of $\alpha_1 + \beta_1$ peaks, while the Si-12Cu20Ce catalyst shows a higher amount of δ_1 peak ascribed to larger clusters and bulk-like CuO species, as revealed also by XRD data (Fig. 2B). This is mainly based on the fact that, in CeO_2-supported copper samples, the proportion of the highest temperature peak with respect to the lowest temperature one usually increases with increasing the copper loading, which is known to lead to segregation of large copper oxide particles. The catalyst with the lowest copper loading (Si-3Cu20Ce) shows a higher proportion of α_1 peak than both Si-6Cu20Ce and Si-12Cu20Ce and this fact can be ascribed to the high dispersion of the copper species that are mainly in the form of isolated Cu^{2+}. Nevertheless, Si-3Cu20Ce catalyst also shows a higher proportion of δ_1 peak than Si-6Cu20Ce, attributable to the presence of larger clusters. However the very low copper amount of this sample suggests that this copper should be well dispersed on the support, so the δ_1 peak could be ascribed to the simultaneous reduction of both iron and copper species. Very small amount of iron are in fact present in the raw clay [20]. This fact is corroborated by the quantitative H_2 consumption (Table 2), where the H_2/Cu molar ratio is higher than 1 in all cases, especially in the two catalysts with the lowest copper content.

In the case of the catalysts supported on SiZr-PCH (Fig. 4B and Table 2), H_2-TPR profiles only show three overlapped peaks between 140 °C and 290 °C. The first one, denoted as α_2, has

been attributed to the hydrogen consumption of weakly bonded oxygen ions of isolated copper species located on the surface oxygen vacancies, the second one, denoted β_2 peak, can be related to the hydrogen consumption of the interfacial oxygen ions of small copper clusters beside the surface oxygen vacancies [57]. The third peak, here named γ_2, can be ascribed to the concomitant reduction of both copper oxide in solid solution in the ceria lattice in addition with the reduction of large clusters and bulk-like CuO. Previous researchers described that the presence of zirconium in the structure produces an increment of the oxygen vacancies favoring the redox behavior in the catalytic system [57,58]. In our case it seems that α_2 and β_2 peaks have a reduction temperature at least 20 °C higher than the PCH catalysts without zirconia. Similarly to Si-PCH, the proportion of α_2 peak diminishes when the copper increases, suggesting that the amount of isolated copper species decreases for higher copper loading. This fact is accompanied by a slight increase of the proportion of β_2 peak, while the third peaks, γ_2, due to the sum of different reduction sites remain almost constant, as shown in Table 2.

In the reduction process of CuO-CeO_2 based catalysts supported both Si-PCH and SiZr-PCH, it cannot be discarded the presence of hydrogen spillover on the support and of a limited reduction of the very small amount of iron present in the clay, whose contribute cannot be considered negligible in the samples with 3 wt% of copper.

3.1.5. XPS

Surface chemical information of the fresh catalysts was obtained from XPS analysis. C $1s$, O $2p$, Fe $2p$, Cu $2p$ and Ce $3d$ core level spectra were recorded and decomposed to determine the species present on the catalyst surface. Short acquisition times were obliged to avoid photoreduction of Ce and Cu, especially in the case of Cu. No peaks attributable to the presence of surface iron species were

Table 3
Redox parameters of fresh and used Si-xCuyCe and SiZr-xCuyCe catalysts.

Sample	Cu/Ce	Cu $2p_{3/2}$ (eV)	Cu_{red}/CuO	I_{sat}/I_{mp}	Ce^{3+}/Ce^{4+}
Si-3Cu20Ce	0.59	932.5 (29.33%) 935.1 (70.67%)	0.29	0.33	0.39
Si-6Cu20Ce	0.82	932.8 (15.60%) 934.8 (84.40%)	0.15	0.40	0.35
Si-12Cu20Ce	0.84	932.1 (4.70%) 934.2 (95.30%)	0.05	0.46	0.52
SiZr-3Cu20Ce	0.46	932.4 (14.63%) 934.5 (85.37%)	0.15	0.39	0.47
SiZr-6Cu20Ce	0.98	933.1 (17.27%) 935.1 (82.73%)	0.17	0.42	0.54
SiZr-12Cu20Ce	0.94	934.8 (100.0%)	0.00	0.49	0.52
Si-3Cu20Ce-U	0.35	933.5 (69.31%) 935.8 (60.69%)	0.69	0.25	0.29
Si-6Cu20Ce-U	0.87	933.8 (62.76%) 935.7 (37.24%)	0.63	0.31	0.39
Si-12Cu20Ce-U	0.92	933.6 (67.55%) 935.9 (32.45%)	0.68	0.32	0.47
SiZr-3Cu20Ce-U	0.47	932.5 (26.09%) 934.3 (73.91%)	0.26	0.33	0.39
SiZr6Cu20Ce-U	0.71	933.3 (73.06%) 935.5 (26.94%)	0.73	0.25	0.40
SiZr12Cu20Ce-U	1.23	933.3 (45.38%) 935.4 (54.62%)	0.66	0.34	0.51

detected in the investigated samples. Table 3 shows the Cu $2p_{3/2}$ binding energy values and redox parameters for all the samples.

Cu $2p$ core level spectra for fresh catalysts are shown in Fig. 5A. Cu $2p_{3/2}$ signal involves two contributions. The first one, centered about 932.8 eV, is attributed to reduced copper species and a second one, about 934.8 eV, can be ascribed Cu^{2+} species. Moreover it is noticeable the presence of a *shake-up satellite* located about 942.1 eV [59]. The presence of reduced copper species can be elucidated by considering the intensity of the satellite contribution at high binding energy together with the intensity of the main peak (I_{sat}/I_{mp}), this ratio being 0.55 if only CuO is present. Instead, an estimation of the proportion of reduced copper species is done considering the ratio between the area of the main peak and the area of all the peaks including the satellite.
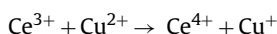
Data included in Table 3 show that all catalysts show a I_{sat}/I_{mp} value lower than that normally observed for CuO (0.55), indicating the presence of partially reduced copper species [60,61] but in the case of samples with 12 wt% of copper a very low reduction degree of Cu^{2+} is observed and the found I_{sat}/I_{mp} values are very close to that of CuO, corroborating XRD and TPR results.

The complex spectra of Ce $3d$ are shown in Fig. 5B and have been deconvolved as proposed by other researchers [62,63]. The core level of Ce 3d signal of ceria is composed by six contributions v, u (Ce $3d^9 4f^2$ O $2p^4$) and v'', u'' (Ce $3d^9 4f^1$ O $2p^5$); v''', u''' (final state of Ce $3d^9 4f^0$ O $2p^6$) assigned to that Ce^{4+} $3d$ final states and four contributions v_0, u_0 (Ce $3d^9 4f^2$ O $2p^5$) and v', u' (Ce $3d^9 4f^1$ O $2p^6$) assigned to Ce^{3+} as a consequence of the hybridization between the Ce 4 levels and the O $2p$ states reveling that both Ce^{3+} and Ce^{4+} species are present in all catalysts.

The amount of Ce^{3+} on the surface has been estimated by the relation:

$$Ce^{3+}(\%) = \frac{S(Ce^{3+})}{S(Ce^{3+} + Ce^{4+})} \times 100 = \frac{S(v) + S(u)}{S(v) + S(u) + S(v') + S(u')} \times 100$$

The quantification of Ce^{3+} species is useful to understand the reaction mechanism of the PROX since it is recognized that Ce^{3+} and Cu^{2+} species suffer a facile electron transfer by the synergistic effect of both species, as follows:

$$Ce^{3+} + Cu^{2+} \rightarrow Ce^{4+} + Cu^{+}$$

favoring the oxidation of CO to CO_2.

The profiles of Ce 3d core level spectra show the coexistence of the typical bands of both Ce^{3+} and Ce^{4+}. The presence of zirconium in the support provokes an increasing of the Ce^{3+}/Ce^{4+} ratio on the surface of the catalyst that suggests that zirconium favors the presence of Ce^{3+} [27].

The Cu/Ce surface ratio increases with the copper content which indicates loss of the dispersion of CuO particles on the support, as revealed by XRD data and H_2-TPR profiles. Nevertheless, these materials present a higher dispersion than the bulk mixed oxides CuO-CeO_2.

The O $1s$ core level spectra show an asymmetric peak that can be decomposed in two contributions at 529.8 and 532.7 eV assigned to oxygen lattice of CeO_2 and to silica, respectively. It is noticeable in the C $1s$ core level spectra the presence of a peak located at 288.6 eV and attributed to carbonate species by the adsorption of the active phase [20].

3.2. Catalytic activity in the CO-PROX reaction

The catalytic activity of CuO-CeO_2 catalysts supported on Si-PCH and SiZr-PCH was evaluated in the CO-PROX reaction under H_2-rich feed, as relevant for the cleanup of reformate streams for PEMFC applications, in the temperature range of 65–190 °C. Reverse water gas shift (rWGS) and methanation reactions were found negligible in our experimental conditions and only CO and H_2 oxidations are the reactions considered in these catalytic tests.

The evolution of the conversion of CO and selectivity towards CO_2 of the catalysts as a function of the reaction temperature is shown in Fig. 6A–B. The CO conversion of all catalysts increases with the reaction temperature, reaching values close to 95–100% between 115–140 °C and it begins to slightly diminish from this temperature to 190 °C. The catalytic results reveal that the catalyst, Si-6Cu20Ce, supported on Si-PCH and with a copper loading of 6 wt% exhibits very high CO conversion values even at very low temperatures: at 65 °C the conversion is 49% and it reaches 100% at 115 °C, keeping constant at this value till 190 °C, the highest tested temperature. Also the catalyst SiZr-6Cu20Ce, supported on SiZr-PCH, displays very good catalytic performances being active in the CO-PROX reaction similarly to Si-12Cu20Ce. The SiZr-12Cu20Ce catalyst and those containing the lowest amount of copper (3 wt%), show a lower CO conversion percentage over all the studied
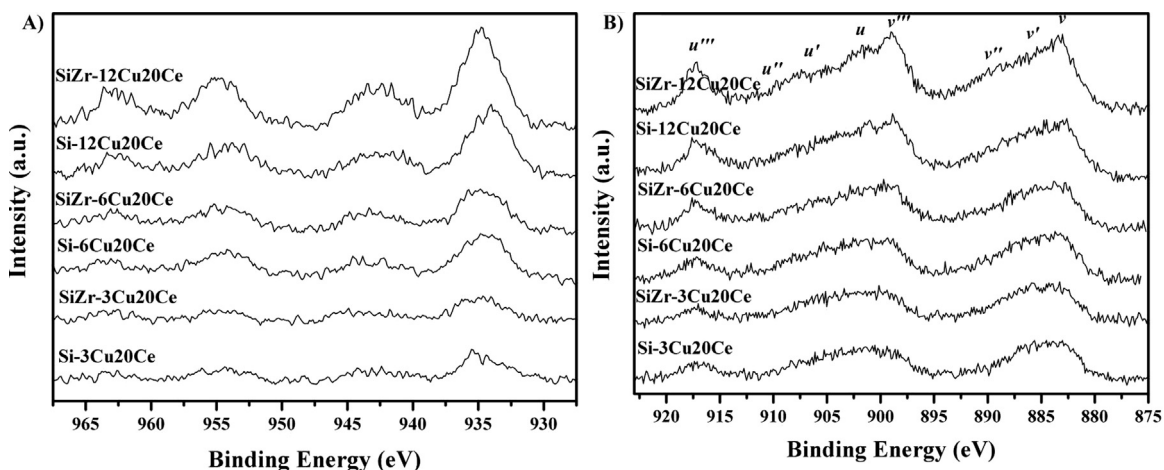
Fig. 5. (A) Cu *2p* core level spectra of Si-*x*Cu*y*Ce and SiZr-*x*Cu*y*Ce catalysts; (B) Ce *3d* core level spectra of Si-*x*Cu*y*Ce and SiZr-*x*Cu*y*Ce samples.

temperature range. The surprising very high conversion values in a large range of temperature for the sample Si-6Cu20Ce could be ascribed to the larger amount of CuO-CeO$_2$ interfacial sites, which has been reported in the literature as the active sites in the CO-PROX reaction, due to the high dispersion and low particle size both CuO and CeO$_2$, as reported in XRD data (Fig. 2B–C), H$_2$-TPR and textural properties (Table 1).

In general, the catalysts supported on Si-PCH exhibit a higher conversion values than that of SiZr-PCH ones. This fact can be ascribed to the fact that the reduction process of Cu species supported on Si-PCH occurs at a temperature lower than on SiZr-PCH, as described in Section 3.1.4 (Fig. 4A–B).

Concerning the selectivity to CO$_2$, it depends on the competition between CO and H$_2$ oxidation. The hydrogen oxidation rate increases faster with increasing temperature than the CO oxidation, because the activation energy of the H$_2$ oxidation is larger than the energy of CO oxidation. Therefore, the amount of O$_2$ consumed by H$_2$ oxidation increases with increasing temperature. In this sense, active sites for hydrogen oxidation were proposed to be related to reduced copper sites, which are formed on top of the copper oxide particles during the course of the interaction of the catalyst with the reactant mixture at a temperature (typically above 100 °C) higher than that required for the formation of Cu$^+$ sites at the interfacial region [64]. This can be correlated with the reduction capability

detected by H$_2$-TPR and typically catalysts that appear more selective for the process are those in which such reduction occurs at higher temperatures during the course of the TPR process.

Otherwise with regard to the selectivity to CO$_2$, all catalysts present a similar trend, with values very close to 100% until 90 °C and a gradual diminution at higher temperatures due to the competitive oxidation of H$_2$, that starts to be thermodynamically favorable at high temperatures [65].

In order to evaluate the modification of the redox properties of the active phase during the catalytic test, the sample were investigated by XRD and XPS techniques after one cycle of catalytic activity.

X-ray diffractograms of the used catalysts (Fig. 7) reveal that the catalysts with a lower copper loading (3 and 6 wt%) exhibit a diffraction pattern almost superimposable to that before catalysis. In the case of catalysts with the highest copper loading (Si-12Cu20Ce and SiZr-12Cu20Ce), the diffraction lines of CuO phase seem to disappear and new diffraction lines located at 43.5 and 50.4° in 2θ, associated to Cu(0) (PDF-ICCD 00-004-0836) arise, suggesting that, under CO-PROX operating conditions, bulk CuO reduces to metallic copper in irreversible way [66].

XPS spectra of Cu 2p core level signal for the catalysts after one cycle of CO-PROX can be decomposed into two peaks (Fig. 8A) with a general decrease of the *shake-up* satellite related with Cu^{2+} species, that leads to an increasing of the Cu$_{red}$/CuO ratio and a decreasing of the I_{sat}/I_{main} ratio. This fact is very pronounced for the samples
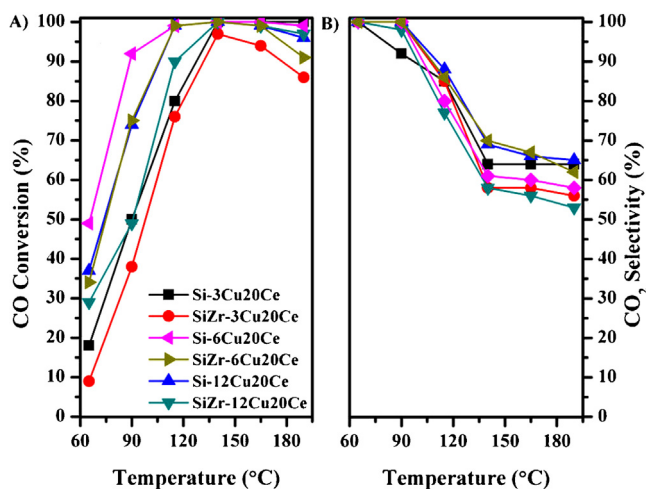

Fig. 6. (A) CO conversion and (B) selectivity toward CO$_2$ as a function of the temperature of Si-*x*Cu*y*Ce and SiZr-*x*Cu*y*Ce catalysts. Operating conditions: GHSV = 22,000 h^{-1}, λ = 2, 1.25% CO, 1.25%O$_2$, 50% H$_2$, He balance (%vol).
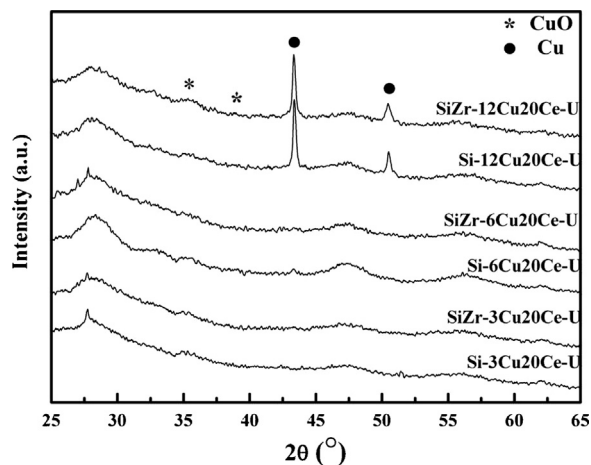

Fig. 7. XRD patterns of Si-*x*Cu*y*Ce and SiZr-*x*Cu*y*Ce catalysts after one cycle of CO-PROX activity.
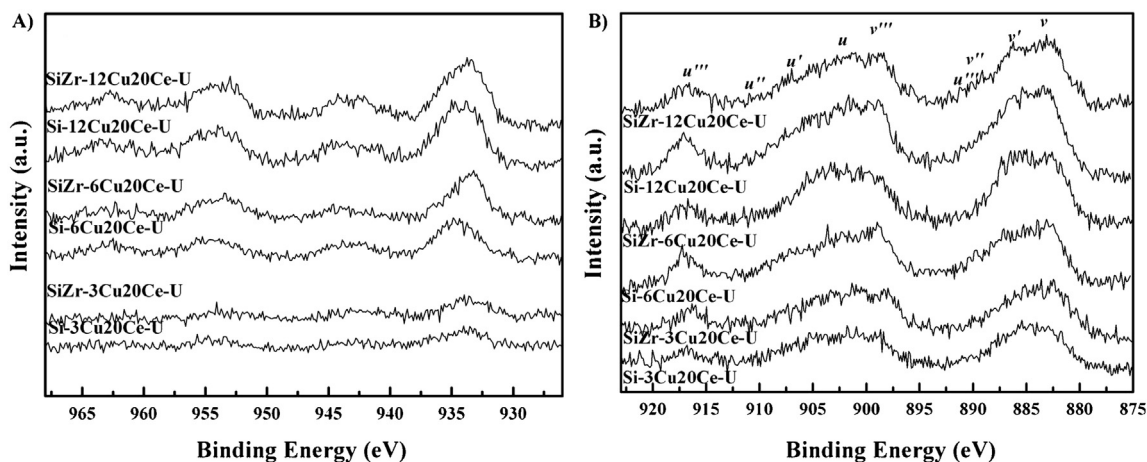
Fig. 8. (A) Cu *2p* core level spectra and (B) Ce *3d* core level spectra of Si-*xCuyCe* and SiZr-*xCuyCe* used catalysts.

containing 12 wt% of copper, suggesting that a large amount of CuO species has been reduced under the H_2-rich feed and corroborating the XRD results of the used catalysts, where the presence of Cu(0) was clearly detected. On the contrary, neither the I_{sat}/I_{mp} ratio nor the Cu_{red}/Cu_{tot} one change significantly after testing the samples with 3 and 6 wt% of copper. In addition, the Ce 3d region (Fig. 8B) shows similar reduction degree than that obtained for the fresh catalysts, which confirms the high stability in the CO-PROX reaction of these catalysts in respect with the 12 wt% Cu-based samples.

Finally, a durability test was performed on the sample with the best catalytic performances, Si-6Cu20Ce (not shown). The reaction was monitored for 72 h maintaining the temperature constant at 115 °C, using GHSV = 22,000 h^{-1}; $\lambda = 2$; 1.25% CO, 1.25% O_2, 50% H_2, He balance (vol.%). The catalyst showed a diminution of CO conversion from 99% to 95% within the first 5 h, remaining stable for the further operation time.

3.2.1. CO-PROX reaction: influence of CO_2 in the feed

Since the reformate H_2-rich stream usually contains carbon dioxide, the effect of the addition of 15 vol.%. CO_2 to the mixture feed stream was studied in the CO-PROX reaction (Fig. 9A–B). As expected, the presence of CO_2 adversely affects the catalytic performance of the studied systems. Results reveal that the CO conversion of all the samples shifts towards higher temperatures (about 20 °C).
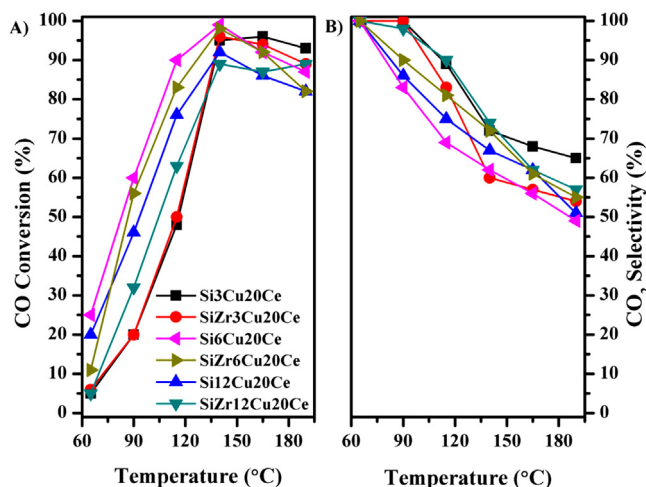

Fig. 9. (A) CO conversion and (B) selectivity toward CO_2 as function of the temperature of Si-*xCuyCe* and SiZr-*xCuyCe* catalysts. Operating conditions: GHSV = 22,000 h^{-1}, $\lambda = 2$, 1.25% CO, 1.25%O_2, 50% H_2, 15% CO_2, He balance (%vol).

In this sense, previous researchers have pointed out that the presence of a high CO_2 content in the feed produces a competitive adsorption between CO and CO_2 by the active sites located on the interface CuO-CeO_2 sites. Moreover, CO_2 interacts with Cu^+ species forming Cu^+-carbonyl that produces a blockage of the active sites and/or leads to the inhibition of oxygen mobility upon formation of carbonates type species (hydrogen carbonate, bidentate carbonate) [67]. Recently, Di Benedetto et al. [68] have established that CO_2 is chemisorbed onto both the ceria and CuO-CeO_2 catalysts, suggesting that its inhibiting effect is due to the formation of stable surface species which can be desorbed at higher temperatures, corroborating the catalytic results. Therefore the CO_2 desorption seems a key factor in the catalytic activity.

In order to determine the influence of CO_2 in H_2-rich feed, temperature programmed desorption of CO_2 (CO_2-TPD) was performed (Fig. 10A–B). All CO_2-TPD profiles present a broad peak that increases with the copper loading in both Si-PCH and SiZr-PCH supports, with a maximum centered between 105 °C and 115 °C, showing similar profiles that have been reported in the literature [66,68,69], pointing out that the CO_2 desorption is attributable to the interaction of this molecule with highly dispersed Cu^{2+} ions strongly interacting with the ceria, species which are claimed as active centers for CO-PROX reaction. Moreover CO_2-TPD profiles can explain how the temperature of CO_2 desorption is related with the catalytic behavior. The temperature range in which CO_2 is desorbed from the catalysts is 80–130 °C and it is coincident with the range in which the CO-PROX reaction is active. In fact, the activity in the PROX reaction increases when CO_2 is desorbed from the active site, in this case at about 105–115 °C, allowing conversion values close to 95% at 140 °C for all the studied catalysts.

3.2.2. CO-PROX reaction: Influence of CO_2 and H_2O in the feed

Finally, in order to simulate the real operation conditions of a PEMFC feeding from water gas shift reaction, both 15 vol.% CO_2 and 10 vol.% H_2O were simultaneously added to the feed stream, since these species are present in significant amount in the reformate gas and are also the reaction products (Fig. 11A–B). The catalytic activity falls down for the catalysts in the whole temperature range, drastically diminishing the CO conversion. Water has been found to enhance the CO oxidation activity over Au-based catalysts [70], while a substantial adverse effect has been observed for CuO-CeO_2 catalysts [69]. In this sense, it is assumed that the decrease of the catalytic activity with H_2O in the reactant feed can be ascribed to the blockage of the adsorbed molecular water of the active sites. However, the influence of water varies with one support to another. The catalytic results shown in this study are disaccording with previous
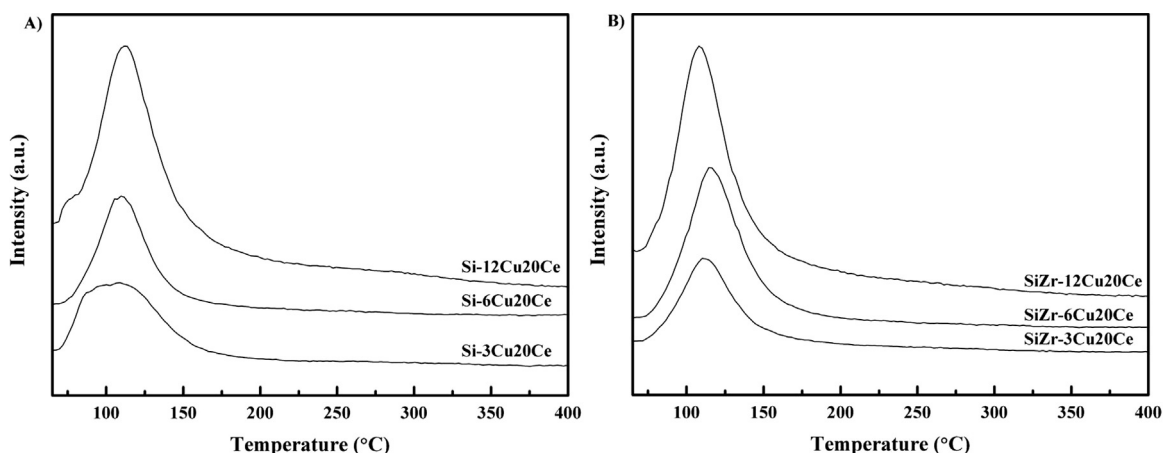
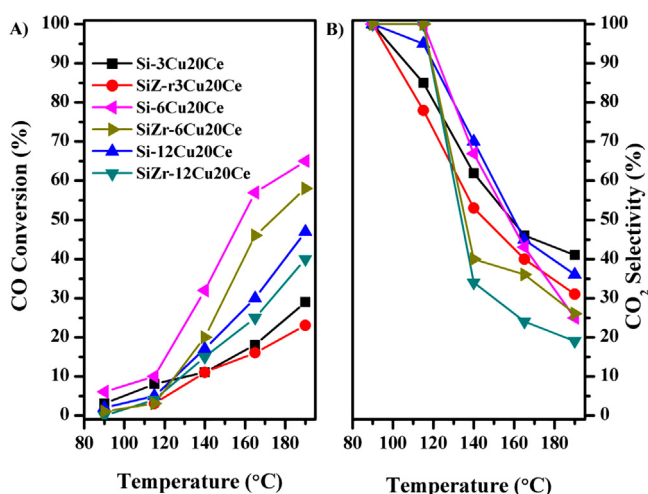**Fig. 10.** CO_2-TPD profiles of the samples: (A) SixCuyCe and (B) SiZrxCuyCe.

Fig. 11. CO conversion (A) and selectivity toward CO_2 (B) as a function of the temperature of Si-xCuyCe and SiZr-xCuyCe catalysts. Operating conditions: GHSV = 22,000 h^{-1}, λ = 2, 1.25% CO, 1.25%O_2, 50% H_2, 15% CO_2, 10% H_2O, He balance (vol.%).

results reported for CuO-CeO$_2$ mixed oxides, which suggests that the blockage of the active centers by the adsorption of H_2O can be influenced by the physical and chemical properties of the support. In the case of PCH-based catalysts, the presence of a relatively high content of hydroxyl and silanol groups in the pillars, mainly in the layers of montmorillonite, favors the formation of hydrogen bonds between the clay layers and water. This fact, together with the high microporosity of the catalysts (Table 1), produces a hindrance for the access of the CO molecules to the active sites.

4. Conclusions

Two porous clay heterostructures (PCHs) were synthesized as support for CuO-CeO$_2$ active phase and used as catalysts in the preferential oxidation of CO to CO_2 in excess of hydrogen. The use of pillars of silica or silica-zirconia inserted in the interlayer space of a montmorillonite clay provides a high surface area support that can favor the dispersion of both CuO and CeO$_2$ active phases, leading to the formation of a high amount of copper-ceria interfacial sites, responsible for a very high catalytic activity in the CO-PROX reaction, comparable to that based on precious metal catalysts. The catalytic behavior of these catalysts showed very interesting conversion values under H_2-rich stream, with a maximum of activity for the catalyst Si-PCH with 6 wt% of copper. This sample reached

almost 50% of CO conversion already at 65 °C and close to 100% at 115 °C. In any case all the catalysts displayed a high selectivity at low temperatures, which are the most interesting for PEMFCs technological applications. Moreover, these catalysts exhibited a high resistance to the addition of CO_2 in the feed, most probably for the presence of isolated very small Cu^{2+} clusters in close contact with CeO_2, as evidenced by H_2-TPR and XPS analysis, species which are claimed as active centers for CO-PROX and that are known to weakly interact with CO_2. The addition of H_2O in the feed provoked a drastic decrease in the catalytic activity probably due to the hard interaction between the catalytic supports Si-PCH and SiZr-PCH and water, hindering the access of CO molecules to the active centers.

The very good performance shown by this class of catalysts in the CO-PROX reaction, prompt us to modify the hydrophilicity of the silica and silica-zirconia pillared clays to achieve higher conversion and selectivity values also when water is added to the feed stream and studies are in progress on this topic.

Acknowledgments

References

[1] M.P. Woods, P. Gawade, B. Tan, U.S. Ozkan, Appl. Catal. B 97 (2010) 28–35.
[2] E. Moretti, M. Lenarda, L. Storaro, R. Frattini, P. Patrono, F. Pinzari, J. Colloid Interface Sci. 306 (2007) 89–95.
[3] P.G. Gray, J.C. Frost, Energy Fuels 12 (1998) 1121–1129.
[4] A. Mishra, R. Prasad, B Chem. React. Eng. Catal. 6 (2011) 1–14.
[5] J.R. Rostrup-Nielsen, J. Sehested, J.K. Norskov, Adv. Catal. 47 (2002) 65–193.
[6] Q. Fu, H. Saltsburg, M. Flytzani-Stephanopoulos, Science 301 (2003) 935–938.
[7] M. Kuriyama, H.S. Tanaka, I. Ito, T. Kubota, T. Miyao, S. Naito, K. Tomishige, K. Kunimori, J. Catal. 225 (2007) 39–48.
[8] I. Rosso, C. Galletti, G. Saracco, E. Garrone, V. Specchia, Appl. Catal. B 48 (2004) 195–203.
[9] O. Pozdnyakova, D. Teschner, A. Wootsch, J. Kröhnert, B. Steinhauer, H. Sauer, L. Toth, F.C. Jentoft, A. Knop-Gericke, Z. Paál, R. Schlögl, J. Catal. 237 (2006) 17–28.
[10] A. Beck, A. Horvath, G. Stefler, M.S. Scurrell, L. Guczi, Top. Catal. 52 (2009) 912–919.
[11] L. Storaro, M. Lenarda, E. Moretti, A. Talon, F. Porta, B. Moltrasio, P. Canton, J. Colloid Interface Sci. 350 (2010) 435–442.
[12] L. Wang, J. Chen, A. Patel, V. Rudolph, Z. Zua, Appl. Catal. A 447–448 (2012) 200–209.
[13] Y.F. Han, M.J. Kahlich, M. Kinne, R.J. Behm, Phys. Chem. Chem. Phys. 4 (2002) 389–397.

[14] S. Ito, H. Tanaka, Y. Minemura, S. Kameoka, K. Tomishige, K. Kunimori, Appl. Catal. A 273 (2004) 295–302.

[15] C. Galletti, S. Specchia, G. Saracco, V. Specchia, Ind. Eng. Chem. Res. 47 (2008) 5304–5312.

[16] D. Gamarra, A. Hornés, Z. Koppány, G. Munuera, J. Soria, A. Martínez-Arias, J. Power Sources 169 (2007) 110–116.

[17] Z. Wu, H. Zhu, Z. Qun, H. Wang, J. Ding, L. Huang, J. Wang, Fuel 1004 (2013) 41–45.

[18] X. Li, X.Y. Quek, D.A.J.M. Ligthart, M. Guo, Y. Zhang, C. Li, Q. Yang, E.J.M. Hensen, Appl. Catal. B 123–124 (2012) 424–432.

[19] A. Gurbani, J.L. Ayastuy, M.P. González-Marcos, M.A. Gutiérrez-Ortiz, Int. J. Hydrogen Energ. 35 (2010) 11582–11590.

[20] J.L. Ayastuy, A. Gurbani, M.P. González-Marcos, M.A. Gutiérrez-Ortiz, Int. J. Hydrogen Energ. 35 (2010) 1232–1244.

[21] T. Caputo, L. Lisi, R. Pirone, G. Russo, Appl. Catal. A: Gen. 348 (2008) 42–53.

[22] D.H. Kim, D.R. Park, J. Lee, Int. J. Hydrogen Energ. 38 (2013) 4429–4436.

[23] Z. Liu, R. Zhou, X. Zheng, Catal. Commun. 9 (2008) 2183–2186.

[24] A. Martínez-Arias, A.B. Hungría, G. Munuera, D. Gamarra, Appl. Catal. B 65 (2006) 207–216.

[25] A. Gómez-Cortés, Y. Márquez, J. Arenas-Alatorre, G. Díaz, Catal. Today 133–135 (2008) 743–749.

[26] J. Han, H.J. Kim, S. Yoon, H. Lee, J. Mol. Catal. A: Chem. 335 (2011) 82–88.

[27] A. Arango-Díaz, J.A. Cecilia, E. Moretti, A. Talon, P. Núñez, J. Marrero-Jerez, J. Jiménez-Jiménez, A. Jiménez-López, E. Rodríguez-Castellón, Int. J. Hydrogen Energ. 39 (2014) 4102–4108.

[28] E. Moretti, L. Storaro, A. Talon, R. Moreno-Tost, E. Rodríguez-Castellón, A. Jiménez-López, M. Lenarda, Catal. Lett. 129 (2009) 323–336.

[29] Á. Reyes-Carmona, A. Arango-Díaz, E. Moretti, A. Talon, L. Storaro, M. Lenarda, A. Jiménez-López, E. Rodríguez-Castellón, J. Power Sources 196 (2011) 4382–4387.

[30] A. Trovarelli, C. de Leitenburg, M. Boaro, G. Dolcetti, Catal. Today 50 (1999) 353–367.

[31] M. Melchionna, P. Fornasiero, Mater. Today 17 (2014) 349–357.

[32] A. Martínez-Arias, M. Fernández-García, J. Soria, J.C. Conesa, J. Catal. 182 (1999) 367–377.

[33] P. Fornasiero, G. Balducci, R. Di Monte, J. Kaspar, V. Sergo, G. Gubitosa, A. Ferrero, M. Graziani, J. Catal. 164 (1996) 173.

[34] E. Moretti, M. Lenarda, P. Riello, L. Storaro, A. Talon, R. Frattini, A. Reyes-Carmona, A. Jiménez-López, E. Rodríguez-Castellón, Appl. Catal. B 129 (2013) 556–565.

[35] R. DiMonte, P. Fornasiero, S. Desinan, J. Kaspar, J.M. Gatica, J.J. Calvino, E. Fonda, Chem. Mater. 16 (2004) 4273–4285.

[36] Y.K. Hwang, D.K. Kim, A.S. Mamman, S.E. Park, J.S. Chang, Chem. Lett. 36 (2007) 186–187.

[37] J.A. Hernandez, S. Gomez, B. Pawelec, T.A. Zepeda, Appl. Catal. B 89 (2009) 128–136.

[38] S. Varghese, M.G. Cutrufello, E. Rombi, C. Cannas, R. Monaci, I. Ferino, Appl. Catal. A 443–444 (2012) 161–170.

[39] V. Ramaswamy, S. Malwadkar, S. Chilukuri, Appl. Catal. B 84 (2008) 21–29.

[40] A. Galarneau, A. Barodawalla, T.J. Pinnavaia, Nature 374 (1995) 529–531.

[41] H.J. Chae, I.S. Nam, S.B. Hong, Catal. Today 68 (2001) 31–40.

[42] M. Polverejan, Y. Liu, T.J. Pinnavaia, Chem. Mater. 14 (2002) 2283–2288.

[43] M.L. Pinto, J. Marques, J. Pires, Sep. Purif. Technol. 98 (2012) 337–343.

[44] J.A. Cecilia, C. García-Sancho, F. Franco, Micropor. Mesopor. Mater. 176 (2013) 95–102.

[45] E. Caballero, J.M. Fernández-Porto, J. Linares, F. Huertas, E. Reyes, Estud. Geolg. 39 (1983) 121–140.

[46] E. Caballero, E. Reyes, J. Linares, F. Huertas, Miner. Petrogr. Acta 29 (1985) 187–196.

[47] S. Brunauer, P.H. Emmet, E. Teller, J. Am. Chem. Soc. 60 (1938) 309–319.

[48] L. Jelinek, E.S. Kováts, Langmuir 10 (1994) 4225–4231.

[49] S. Poulston, P.M. Parlett, P. Stone, M. Bowker, Surf. Interf. Anal. 24 (1996) 811–820.

[50] E. Moretti, L. Storaro, A. Talon, M. Lenarda, Catal. Commun. 10 (2009) 522–527.

[51] L.G. Schultz, Clay Miner. 17 (1969) 115–137.

[52] K.S.W. Sing, D.H. Everett, R.A.W. Haul, L. Moscou, R.A. Pierotti, J. Rouquerol, T. Siemieniewska, Pure Appl. Chem. 57 (1985) 603.

[53] F. Rouquerol, J. Rouquerol, K. Sing, Adsorption by Powders and Porous Solids, Academic Press, London, 1999, Chapter 13.

[54] M.L. Occelli, Catal. Today 2 (1988) 339–355.

[55] P. Ratnasamy, D. Srinivas, C.V.V. Satyanarayana, P. Manikandan, R.S. Senthil Kumaran, M. Sachin, V.N. Shetti, J. Catal. 221 (2004) 455–465.

[56] P. Bera, K.R. Priolkar, P.R. Sarode, M.S. Hedge, S. Emura, R. Kumashiro, Chem. Mater. 14 (2002) 3591–3601.

[57] Q. Yu, L. Liu, L. Dong, D. Li, B. Liu, F. Gao, K. Sun, L. Dong, Y. Chen, Appl. Catal. B 96 (2010) 350–360.

[58] J.L. Ayastuy, A. Gurbani, M.P. González-Marcos, M.A. Gutiérrez-Ortiz, Int. J. Hydrogen Energ. 37 (2012) 1993–2006.

[59] X. Tang, B. Zhang, Y. Li, Y. Xu, Q. Xin, W. Shen, Appl. Catal. A 288 (2005) 116–125.

[60] G. Avgouropoulos, T. Ioannides, Appl. Catal. B 67 (2006) 1–11.

[61] H.X. Mai, L.D. Sun, Y.W. Zhang, R. Si, W. Feng, H.P. Zhang, H.C. Liu, C.H. Yan, J. Phys. Chem. B 109 (2005) 24380–24385.

[62] P. Burroughs, A. Hamnet, A.F. Orchard, G. Thornton, J. Chem. Soc. Dalton 17 (1976) 1686–1698.

[63] F. Zhang, P. Wang, J. Koberstein, S. Khalid, S. Chan, Surf. Sci. 563 (2004) 74–82.

[64] D. Gamarra, C. Belver, M. Fernández-García, A. Martínez-Arias, J. Am. Chem. Soc. 129 (2007) 12064–12065.

[65] R. DiMonte, J. Kaspar, J. Mater. Chem. 15 (2005) 633–648.

[66] A. Martínez-Arias, D. Gamarra, A.B. Hungría, M. Fernández-García, G. Munuera, A. Hornes, P. Bera, J.C. Conesa, A. Lopez Camara, Catalysts 3 (2013) 378–400.

[67] F. Mariño, C. Descorme, D. Duprez, Appl. Catal. B 58 (2005) 175–183.

[68] A. Di Benedetto, G. Landi, L. Lisi, G. Russo, Appl. Catal. B 142 (2013) 169–177.

[69] G. Avgouropoulos, T. Ioannides, Appl. Catal. A 244 (2003) 155–167.

[70] M. Haruta, M. Date, Appl. Catal. A 222 (2001) 427–437.